Evanescent Microwaves: A Novel Super-Resolution Noncontact Nondestructive Imaging Technique for Biological Applications

M. Tabib-Azar, J. L. Katz, and S. R. LeClair

***Abstract*—Scanning tunneling microscopes (STM) and atomic force microscopes (AFM) are used to study biological materials. These methods, often capable of achieving atomic resolutions, reveal fascinating information regarding the inner workings of these materials. However, both STM and AFM require physical contact to the specimen. In the case of STM the specimen needs to be conducting as well. Here we introduce a new method for imaging biological materials through air or a suitable liquid using decaying or evanescent fields at the tip of a properly designed microwave resonator. This novel method involves the use of an evanescent microwave probe (EMP) and it is capable of imaging a variety of nonuniformities in biological materials including conductivity, permittivity, and density variations. EMP is a noncontact and nondestructive sensor and it does not require conducting specimens. Its spatial resolution is currently around 0.4 μm at 1 GHz. We have used this probe to map nonuniformities in a variety of materials including metals, semiconductors, insulators, and biological and botanical samples. Here we discuss applications of EMP imaging in bone, teeth, botanical, and agricultural specimens.**

***Index Terms*—Biological materials, electromagnetic properties of materials, microwave imaging, material characterization, near-field imaging, super-resolution imaging.**

I. Introduction

SCANNING tunneling microscopy (STM), atomic force microscopy (AFM), scanning near-field optical microscopy (SNOM), and various microwave near-field microscopy methods have become quite popular and have received notable acclaim in recent years [1]–[19] for enabling nano through micro scale imaging of materials. In that context, it is also well known that evanescent electromagnetic fields can be used to surpass the Abbe barrier in microscopy and resolve objects much smaller than the wavelength of the excitation fields [1]–[6]. Toward that end, [6]–[16] we have shown that evanescent microwave probes can achieve a resolution of $\lambda/750\,000$, which at 1 GHz, results in 0.4 μm lateral resolution [8].

Evanescent wave imaging methods are quite powerful, and most of the recent scanning techniques with atomic or near atomic resolutions use some form of evanescent field phenomena. STM, for example, uses evanescent electronic wavefunctions to image atoms at the surface of *metals* or other *conducting materials*. SNOM uses evanescent optical fields to image variations in the refractive index or optical *absorption* with spatial resolutions of 50–100 Å (this is approximately $\lambda/100$, with λ (5000–10 000 Å). AFM uses interactions between near-field electronic wavefunctions and atomic cores to image atoms at the surface of insulators. In all these methods the spatial resolution is essentially limited by the noise in the system for a given probe tip geometry and sensing method.

Evanescent microwave fields were first used by Bethe in calculating the coupling coefficient of microwave waveguides connected to each other through a hole much smaller than the microwave wavelength [1]. Ash is credited with generating evanescent microwave fields in a very elaborate test rig to demonstrate that these fields can be used to resolve metallic features on the order of $\lambda/100$ [3]. Several research groups, including our own, have used a 2-D microstripline quarter-wavelength resonator in the characterization of semiconductors with $\lambda/1000$ resolution [4], [6]. The EMP used in our work is a planar structure that readily lends itself to implementation on a silicon cantilever beam. We started working on evanescent microwave probes for imaging applications in the early 90's, and our initial resolution using a microstripline resonator was around 80 μm at 1 GHz [6]. Our current resolution is around 0.4 μm at 1 GHz and 0.04 μm at 10 GHz. As will be discussed later, our probe configuration is based on two-dimensional (2-D) microstripline waveguide geometries. We have shown that a variety of materials ranging from conductors to insulators can be imaged using the EMP [6]–[16]. Our work in microwave super-resolution imaging of biological and botanical specimens, e.g., woods and fruits, has shown that interesting microwave resistivity maps can be obtained and used to study aging and other processes in these materials [12].

For example, EMP can be used to monitor electrical activities in bone samples [15]–[19]. Resorption and remodeling of bone have been attributed to osteocytic cells sensing changes in streaming potentials generated during deformation of the tissue. Thus, measurements of the electro-magnetic properties of such tissues could prove crucial in the development of models to explain bone remodeling. EMP is sensitive to moisture and ionic mineral content such as variations in tooth enamel. EMP is capable of detecting the onset of caries—believed to

Manuscript received August 24, 1999.

M. Tabib-Azar is with the Electrical Engineering and Computer Science Department, Case Western Reserve University, Cleveland, OH 44106 USA.

J. L. Katz is with the Biomedical Engineering Department, Case Western Reserve University, Cleveland, OH 44106 USA.

S. R. LeClair is with the Air Force Research Laboratory, Materials & Manufacturing Directorate, Wright-Patterson AFB, OH USA.

Publisher Item Identifier S 0018-9456(99)09185-8.

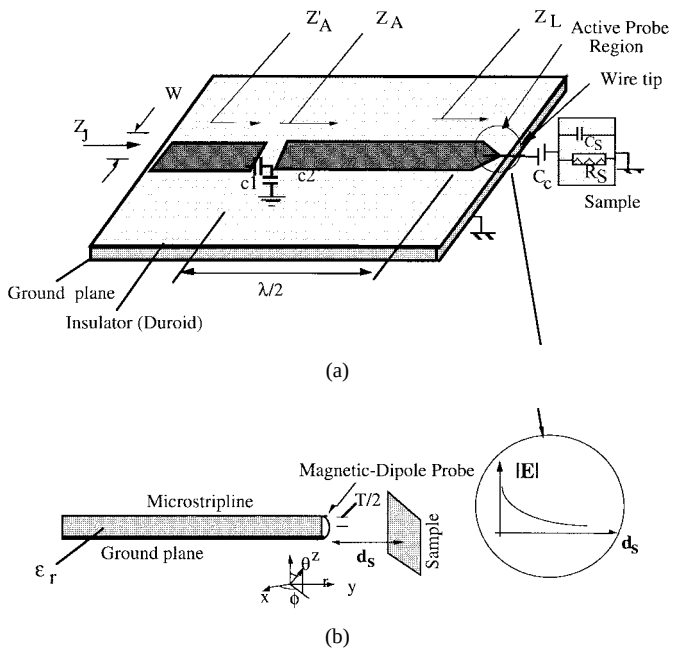

Fig. 1. (a) Microstripline resonator and probe assembly. Evanescent waves extend out of the tapered tip of the resonator. (b) The magnetic dipole probe is modeled as a microstripline with a short length of current carrying wire. The electric dipole probe is shown in (a).

be accompanied by minute surface blemishes with increased moisture and varying degrees of mineralization. Having a microwave power of less than nano-Watts, this unique probe promises to significantly reduce the time-to-detection of cavity formation, enabling timely prevention [15].

II. Operations Principle

EMP principles of operation are explained using a microstripline resonator geometry shown in Fig. 1 [6]–[8]. The reflection coefficient of this resonator is shown in Fig. 2. When an object is placed in the vicinity of the tip of the resonator (Fig. 1), the resonator's reflection coefficient changes as shown in Fig. 2. Both the resonance frequency (f_r) and the quality factor of the resonator (Q) are affected by the presence of the sample. The amount of change in the resonance (Δf_r and ΔQ) depends primarily on the microwave properties of the sample as well as on the distance between the resonator's tip and the sample (d_s), and the tip's effective area (A_{eff}). Keeping A_{eff} and d_s fixed, the tip can be scanned over the sample and variations in the sample's microwave properties can be mapped.

Microwave properties of a material are a function of permittivity, permeability, and free carrier concentration [6]. In most biological tissues, moisture content and ionic species, such as Na^+ and K^+, probably affect the conductivity significantly. These parameters along with density variations, which affect the permittivity, can be mapped using EMP [6]–[16]. Varying signal detection methods can be used to monitor the microwave properties of a sample using an EMP. As can be seen in Fig. 2, one can fix the operation frequency at f_x and monitor the change in the reflection amplitude. f_x is usually

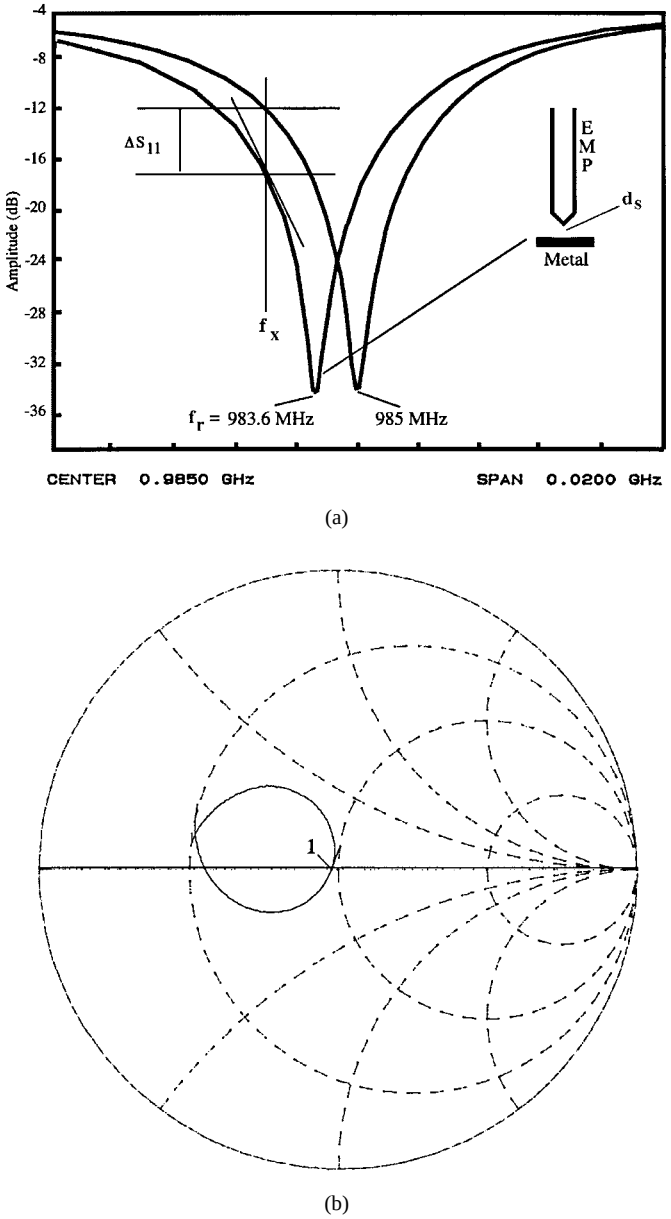

Fig. 2. (a) Presence of a copper plate close to the probe shifts the resonant frequency by 2.4 MHz. ΔS_{11} is the change in the probe's output at f_x. (b) Smith Chart of the resonator. At pointer "1" corresponding to the resonance frequency, the real part of the impedance was 0.125 Ω and its imaginary part was inductive with 21.505 pH inductance as indicated by the network analyzer. The real part became 5.125 Ω while the imaginary part became 911 pH in the presence of the copper plate.

chosen to yield maximum change in the probe's reflection coefficient for a given range of parameters in a sample [7].

Alternatively, one can detect Δf_x directly by using a feedback loop that maximizes the amplitude of the reflection coefficient by changing the operation frequency. Alternatively, one can use a network analyzer and extract the probe parameters from a Smith Chart of the resonator as shown in Fig. 2(b). In another approach, the sample-to-probe distance is varied to keep the reflection coefficient constant at a fixed operation frequency. This method is rarely used in the EMP but is usually used in the routine operation of STM.

Both synchronous and asynchronous detection methods can be used in conjunction with the above methods to map material

nonuniformity. The main difference in the above detection methods is the difference in their signal-to-noise ratios (SNR). We have noticed that operating at a fixed frequency and performing synchronous detection by vertically vibrating the probe above the sample gives the best result and it is also very convenient to implement [7]. In the next section we discuss the experimental set-up used in our EMP measurements.

III. Experimental Set-Up and Procedures

The experimental set-up is shown in Fig. 3 and it is similar to the set-up previously reported [6]–[16]. It consists of a microwave resonator coupled to a feed line (Fig. 1) and connected to a circulator. The resonator was fabricated on a 0.68 mm thick Duroid substrate with $\epsilon_r = 2.2$ using photolithography. The resonator line-width was 2.6 mm and its length was around 10 cm. The circulator in Fig. 3 is also connected to a 0.01–1.05 GHz signal generator, and to a crystal microwave detector. The detector output is a dc voltage proportional to the magnitude of the reflected wave. This voltage is fed to an amplifier and thence to a lock-in amplifier. The probe is mounted vertically over a x-y stage [Fig. 2(b)]. Both the x-y stage and the frequency generator are controlled by a computer. The computer also acquires data from the lock-in amplifier. In synchronous measurements, either the probe or the sample is vibrated at $\approx$ 100 Hz. Although a bit more involved, both from the design and construction point of views, vibrating the probe is better than vibrating the sample. Specially in the case of a large sample, it is not possible to uniformly vibrate the sample without affecting the probe performance.

During measurements the sample was fixed on the x-y stage. We implemented a distance monitoring using a fiber-optic sensor, or another EMP operating at a different frequency, to monitor the probe-to-sample distance and keep it fixed if desired. As we mentioned before, since the probe tip does not contact the sample, the sample's surface can have a variety of characteristics, to include being sticky or immersed in a dielectric fluid. To improve the spatial resolution of the EMP, a wire with a pointed etched tip is usually attached to the tapered portion of the resonator [8]. We have shown that the EMP's spatial resolution is directly determined by the geometry of this wire's tip, i.e., a smaller tip improves spatial resolution. Moreover, the tip-to-sample distance should be made as small as possible.

In our measurements we used a 12 bit, 100 KHz National Instrument Data Acquisition board along with their Lab-View Software to control the stepper motors, to acquire the data and to construct the pseudo-colored 2-D images.

According to our previous findings, a well-designed 2-D stripline microwave probe should detect metallic features of less than 0.1 μm size in a dielectric background or dielectric lines of the same feature size in a metallic background at 1 GHz [7]. Again, the spatial resolution of the probe was theoretically found to be directly proportional to its tip size, and it is strongly affected by the distance between the tip and the sample. The conductivity resolution of this probe was estimated to be $10^{-2}\sigma_s$ in metals and $10^{-4}\sigma_s$ in semiconductors, and its permittivity resolution is $10^{-3}\epsilon_s$ in dielectrics. Experimentally we have found a spatial resolution of $\lambda/750\,000$ (0.4 μm) and conductivity resolution of $10^{-1}\sigma_s$

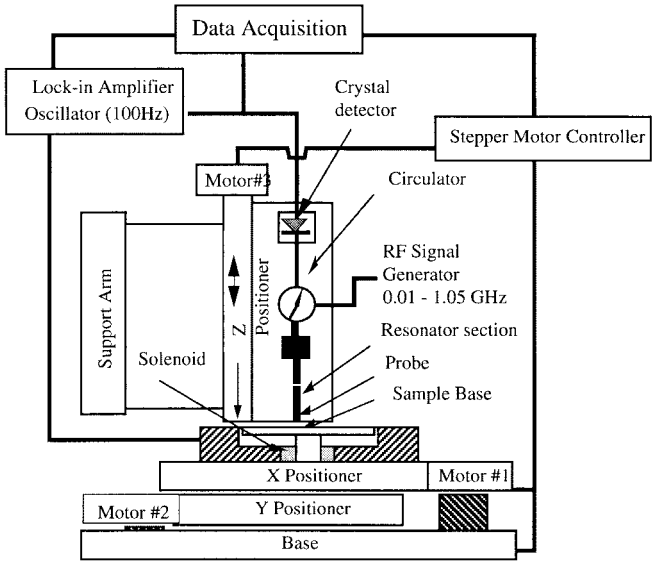

(a)

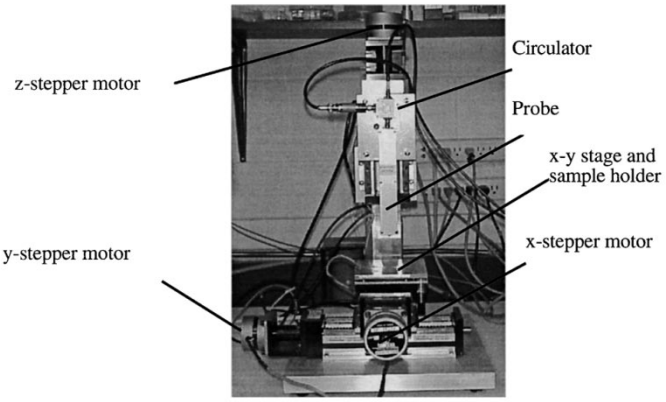

(b)

Fig. 3. (a) Schematic of the experimental set-up and (b) probe housing and the x-y-z scanner arrangement.

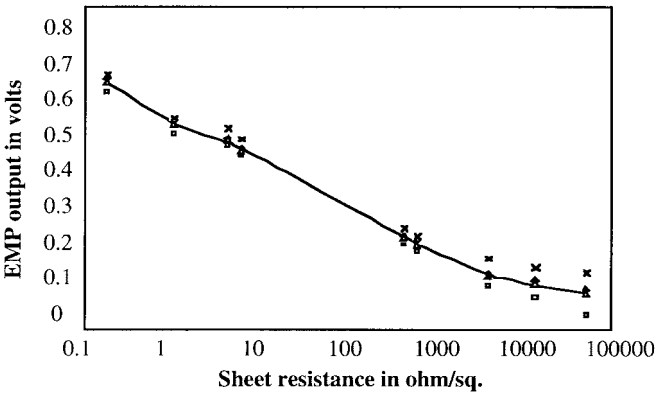

Fig. 4. Evanescent microwave probe calibration using silicon samples with different resistivities. Different symbols in this graph corresponds to repeated measurements that were performed to study the reproducibility of the EMP output.

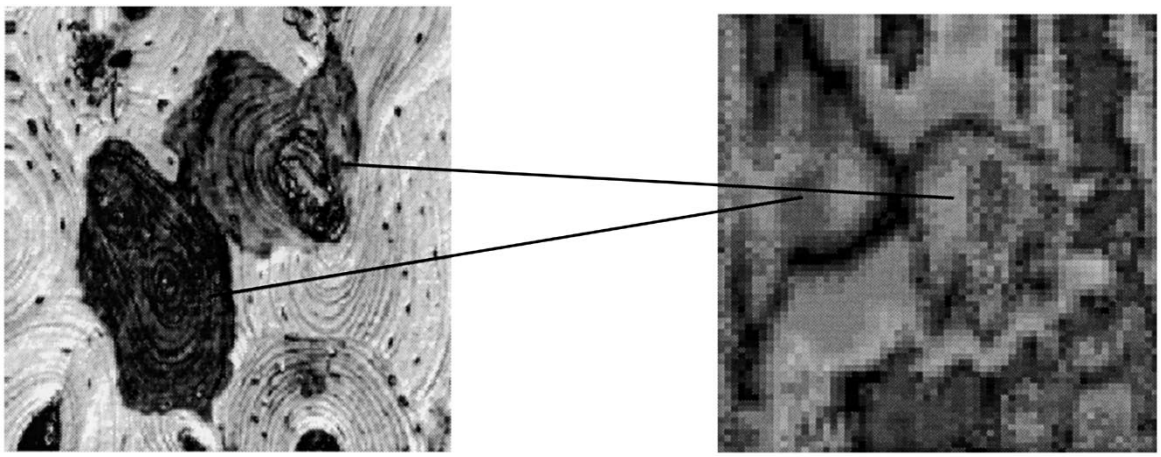

(a) (b)

Fig. 5. (a) 400 MHz (120 aperture burst mode) SAM micrograph (resolution approximately 2.5 μm) micrograph of a portion of human femoral cortical bone cut transverse to the bone axis. The two center osteons show darker grey levels than the surrounding bony tissue. (b) 1 GHz SEMP scan over the same area shown in (a). The voltage across the image varied by 197 mV (resolution was approximately 10 μm).

in metals, $10^{-4}\sigma_s$ in semiconductors, and $10^{-3}\epsilon_s$ in dielectrics at 1 GHz [7].

IV. Experimental Results and Discussion

To perform quantitative mapping of conductivity, we calibrated the probe over a wide range of sheet resistance, from 0.24 Ω/square to 65 kΩ/square. We used a Signatone 4-point probe together with Keithley 182 Sensitive Digital Multimeter and 202 Programmable Current Source to measure the sheet resistance of different samples. With this highly sensitive setup, a change of 10^{-4} in surface resistance could be detected, and the deviation was below 2%. For each sample, a fiber optic distance sensor was used to adjust the probe-to-sample distance to be exactly 2 μm to ensure the reproducibility.

Silicon wafers with different doping levels were used for calibration of EMP. Fig. 4 shows the calibration results [8]. EMP output monotonically decreased as a function of silicon's surface resistance. The accuracy of our measurement was better than 6% for samples of low resistivity, and became larger (50%) for high resistivity samples. This was expected since it is well known that four-point probe is not suitable for measuring high resistivity samples.

Biological Specimens: Specimens of control bone were obtained from the mid-shaft of a femur from a human cadaver. Specimens of trabecular bone were obtained from the middle of the femoral condyle of another human femur. In both cases, the specimens were cut with a diamond knife slowly under running water. They were then polished with successive finer and finer paper down to 600 grit. The specimens were maintained in fluid in a freezer until thawed for use with a scanning acoustic microscope (SAM) and EMP [15]–[19].

The SAM studies were done using the 400 and 600 MHz burst mode lenses, nominal resolutions of 2.5 and 1.7 μm, respectively. Since the focal lengths in each case were much less than 1 mm, a drop of water was sufficient to couple the lens to the bone specimen by surface tension. The specimen is leveled, via the software resident with the UH3, so that the acoustic beam is everywhere perpendicular to its surface. Scan

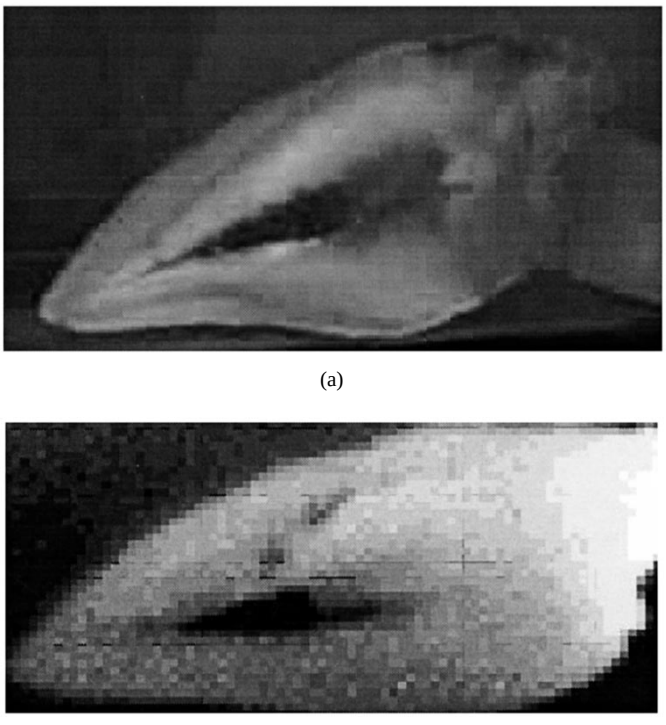

(a)

(b)

Fig. 6. (a) Optical image and (b) evanescent microwave image of a tooth sample.

lengths ranged from 100 μm to 2 mm. Three control knobs determined the range of image resolution (i.e., shades of gray); attenuation, intensity and contrast. It was imperative that these parameters be carefully controlled to avoid saturation of the signals.

The SAM apparatus did not provide an internal calibration to determine the value of acoustic impedance from the reflection coefficient. A calibration system was developed based on correlating the voltage recorded in the receiving mode and the reflection coefficient measured for seven well-defined materials whose acoustic impedances and elastic moduli were measured independently by ultrasonic wave propagation. Thus,

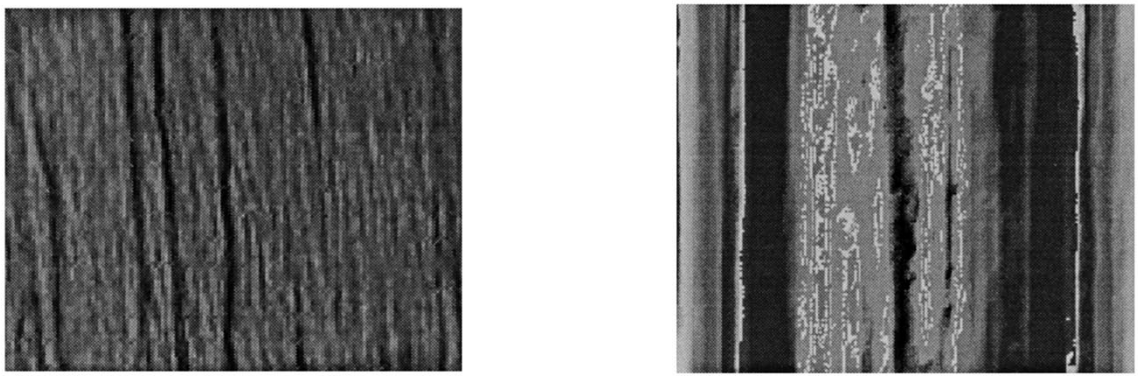

(a) (b)

Fig. 7. (a) Optical image of a balsa wood (2×1 cm^2). (b) EMP scan of the same balsa wood clearly showing regions containing moisture (white areas).

it was possible to determine the value of Z of any desired point on the specimen. $Z = \rho v$ and elastic modulus $E = \rho v^2$ are closely related, where ρ is the density. Using the calibration curves, it was then possible to obtain values of E for selected areas of both the cortical and trabecular bone. The same specimens of both cortical and trabecular bone were then scanned over the same areas as with SAM using the EMP at 1 GHz (nominal resolution here was 10 μm).

Fig. 5 is a 400 MHz (120° aperture burst mode) SAM micrograph of a portion of human cortical bone cut transverse to the bone axis. The same three key observations were reported on related specimens at 600 MHz (120° aperture burst mode) [20] that are observed here. This includes the outermost lamella of each osteon having a darker shade of gray (lower elastic modulus); adjacent moduli alternate in their shades of gray—dark, light, dark, etc.—implying compliant, stiffer compliant and lamellar properties. The outermost lamellae of adjacent abutting osteons appear to have their shades of gray interdigitated, indicating similar elastic properties although their structures are quite distinct as confirmed by scanning electron microscope (SEM) studies.

The specific area mapped on Fig. 5 has an interesting feature, which is why this specimen was chosen for the initial study using the EMP as well. The two central haversian systems (osteons) exhibit much darker gray levels than the neighboring systems. This is presumed to be associated with lower densities of both the organic and inorganic constituents of bone and/or alterations in their orientations, the types of variations in material properties that affects the resistivity recorded by EMP. Fig. 5 also shows the EMP scan over an area close to that of the SAM image. The voltage varied by 197 mV across the image. The circular-like portion indicated by the arrow-corresponds to the very dark osteon observed on the SAM image. Since both the SAM and EMP studies were done with the specimen maintained in a fluid environment, the studies can be repeated with little or no changes in the specimen structure and material properties. Thus, the scans are mapping the specimen's respective intrinsic properties such as elasticity and microwave resistivity.

Fig. 6 shows both the optical and EMP images of a tooth cross-section. EMP is capable of detecting the dark portion of the tooth with cavity. We are currently extending these studies to detect incipient caries without obvious clinical and radiographic manifestation in human teeth. EMP is sensitive to moisture, and ionic mineral content variations in the tooth enamel. Hence, it is capable of detecting the onset of caries believed to be accompanied by minute surface blemishes with increased moisture and varying degrees of mineralization.

Fig. 7 shows an optical image of a balsa wood and its corresponding EMP image. Regions of higher moisture content in this balsa wood can be seen as white regions in the EMP image. With more refined EMP measurements it should be possible to detect the mineral contents as well as density variations in woods and other similar hierarchical materials.

V. Conclusion and Future Studies

For the first time it has been possible to measure both the elastic and the electrical properties of skeletal tissues at the micrometer level of resolution using SAM and EMP, respectively. The SAM operates at up to 2 GHz with 0.5 μm resolution and EMP operates at up to 10 GHz also with sub-micrometer resolution. The combination of SAM and EMP is also being applied to other biological tissues such as skin, cartilage, etc. As the EMP properties of different tissues are complied it is possible that the probe could be made into a useful imaging tool, complementing X-ray and NMR imaging. EMP imaging also shows promise for detecting moisture and mineral content of botanical and agricultural specimens and it appears that it can be used to detect incipient caries in tooth and to prevent cavity formation by a timely treatment.

References

[1] H. A. Bethe "Theory of diffraction by small holes," *Phys. Rev.*, vol. 66, pp. 163–182, 1944.
[2] R. F. Soohoo, "A microwave magnetic microscope," *J. App. Phys.*, vol. 33, no. 3, pp. 1276–77, 1962.
[3] E. A. Ash and G. Nicholls, "Super-resolution aperture scanning microscope," *Nature*, vol. 237, pp. 510–512, 1972.
[4] R. J. Gutmann, J. M. Borrego, P. Chakrabarti, and W. Ming-Shan, "Microwave scanning microscopy for planar structure diagnostics," *1987 IEEE MTT-S Dig.*, pp. 281–284.
[5] M. Fee, S. Chu, and T. W. Hansch, "Scanning electromagnetic transmission line microscope with sub-wavelength resolution," *Opt. Commun.*, vol. 69, pp. 219–224, 1989.
[6] M. Tabib-Azar, N. S. Shoemaker, and S. Harris, "Non-destructive characterization of materials by evanescent microwaves," *Meas. Sci. Technol.*, vol. 4, pp. 583–590, 1993.

[7] M. Tabib-Azar, G. Ponchak, and S. LeClair, "Theoretical resolution of imaging with evanescent microwave probes," *Rev. Sci. Instrum.*, to be published.
[8] M. Tabib-Azar, D.-P. Su, A. Pohar, S. R. LeClair, and G. Ponchak, "0.4 μm spatial resolution with 1 GHz $\lambda = 30$ cm) evanescent microwave probe," *Rev. Sci. Instrum.*, vol. 70, no. 3, pp. 1725–1729, 1999.
[9] M. Tabib-Azar, "Theoretical resolution of imaging with evanescent microwave probes," submitted for publication.
[10] M. Tabib-Azar, P. S. Pathak, G. Ponchak, and S. R. LeClair, "Nondestructive superresolution imaging of defects and nonuniformities in metals, semiconductors, dielectrics, composites, and plants using evanescent microwaves," *Rev. Sci. Instrum.*, vol. 70, no. 6, pp. 2783–2792, 1999.
[11] M. Tabib-Azar, D. Akinwande, G. E. Ponchak, and S. R. LeClair, "Evanescent microwave probes on high-resistivity silicon and its application in characterization of semiconductors," *Rev. Sci. Instrum.*, vol. 70, no. 7, 1999.
[12] ——, "Novel physical sensors using evanescent microwave probes," *Rev. Sci. Instrum.*, vol. 70, no. 8, 1999.
[13] M. Tabib-Azar, R. Ciocan, G. Ponchak and S. R. LeClair, "Transient thermography using microwave microscope," *Rev. Sci. Instrum.*, vol. 70, 8, 1999.
[14] M. Tabib-Azar and B. Sutapun, "Novel hydrogen sensors using evanescent microwave probes," *Rev. Sci. Instrum.*, vol. 70, no. 9, 1999.
[15] M. Tabib-Azar, M. Mozayeni-Azar, S.-H. You, D.-P. Su, and L. J. Katz, "Electro-mechanical properties of tooth structures and caries at high resolution," in *Proc. 1999 IADR*, Vancouver, B.C., Canada.
[16] J. L. Katz, P. S. Pathak, S. Bumrerraj, and M. Tabib-Azar, "Electro-mechanical studies of skeletal tissues at high resolution," *20th Annu. Int. Conf. IEEE Engineering Medicine Biology Society*, 1998.
[17] P. Pathak, M. Tabib-Azar, and G. Ponchak, "An evanescent microwave probe for super resolution nondestructive imaging of metals, semiconductors, dielectrics, composites and biological specimens," in *Proc. 1998 Conf. Nondestructive Testing*, Anaheim, CA, 1998.
[18] J. L. Katz, M. Tabib-Azar, S. Bumrerraj, and P. S. Pathak, "Electro-mechanical properties of mineralized tissues at high resolution," in *Proc. 1998 IADR*, Nice, France, June 24–27, 1998.
[19] ——, "Electro-mechanical studies bone tissue at micrometer resolution," in *Proc. 3rd World Congr. Biomechanics*, Aug. 2–8, Hokkaido Univ., Sapporo, Japan, 1998.
[20] J. L. Katz and A. Meunier, "Scanning acoustic microscopy studies of the elastic properties of osteons and osteon lamellae," *J. Biomech. Eng.*, vol. 115, pp. 543–548, 1993.

M. Tabib-Azar, photograph and biography not available at the time of publication.

J. L. Katz, photograph and biography not available at the time of publication.

S. R. LeClair, photograph and biography not available at the time of publication.